LAWS GOVERNING THE INTERACTION OF LOW-ENERGY ELECTRONS WITH MASSIVE GASEOUS ABSORBERS

V. E. Ivanov and N. K. Osipov

UDC 533.9(201)

Laboratory investigations of the characteristics of the transfer of electrons with initial energies of 0.6-4 keV in massive (thick)* targets (Al, Cu, Ge, Au), carried out in [1, 2], showed a considerable difference between the penetration curves for this case and analogous curves for free (thin) targets [1-5]. The reasons for this difference lie primarily in the properties of the interactions of low-energy electrons with the material of a massive absorber; for these there is a considerable increase in the probabilities of scattering of electrons through larger angles and large discrete energy losses as a result of single collisions. For the case of massive targets, these effects lead to favorable conditions for the formation of intensive beams of backscattered electrons. The presence of such beams shows that in the theoretical analysis of transfer processes in thick absorbers it is inadmissible, in principle, to use approximations for continuous and small losses of energy and scattering through small angles.

For these reasons, it is of interest to simulate the process of electron transfer in massive absorbers without the restrictions of those approximations. The purpose of the present paper is to describe a simulation study of the characteristics of the transfer of electrons with low energy ($E_0 \leqslant 1$ keV) in a semiinfinite gaseous medium, depending on the initial parameters of the primary electron beam. The resulting penetration curves and the integral path lengths calculated on the basis of those curves characterize directly both the size of the dissipation zone for the energy of the primary electron beam and the effective depth of the beam's penetration into the absorber. The integral path lengths constitute a convenient physical parameter for constructing normalized dissipation functions describing the in-depth distribution of the energy stored in the absorber. The use of the path lengths as normalizing parameters enables us to compare the transfer characteristics obtained in experiments using various types of targets. In addition, the simulation of electron-transfer processes under conditions of massive absorption (scattering through large angles, multiple scattering, large energy losses) should facilitate as far as possible a more thorough understanding of the connection between the observed integral characteristics and the quantities representing the elementary scattering processes. A gaseous absorber was chosen as the object of investigation because there is great interest in the study of the characteristics of scattering of low-energy electrons in gaseous media for plasma physics, in particular for applied problems in space-physics and astrophysics profiles.

Model of the Transfer. The electron trajectories were simulated in a three-component gaseous medium, using the method of statistical tests. The use of the scheme of "individual" collisions, which consists in the simulation of each individual interaction, enabled us to take account properly of the probabilistic character of the individual scattering events. As is known, the scheme of individual collisions in the description of the particle-transfer process makes it possible to describe transfer processes with a minimum number of simplifying assumptions concerning the scattering of the particles. The systematic error of the results obtained will depend mainly on the errors of the differential and integral scattering cross sections used. The process of calculating the electron trajectories consists of the following main stages: a) determining the free path length and the coordinates of the point at which the collision took place; b) determining the kind of gas by which the electrons were scattered and the specific type of interaction; c) determining the scattering angle, the energy losses, and the new parameters of the electron after the interaction.

*By a massive (thick) absorber (target) we shall mean an absorber in which the "thickness" of the target (in $g \cdot cm^{-2}$) is much larger than the integral length of the electron path.

Krasnoyarsk. Translated from Zhurnal Prikladnoi Mekhaniki i Tekhnicheskoi Fiziki, No. 1, pp. 20-27, January-February, 1981. Original article submitted December 26, 1979.

 0021-8944/81/2201-0016$07.50

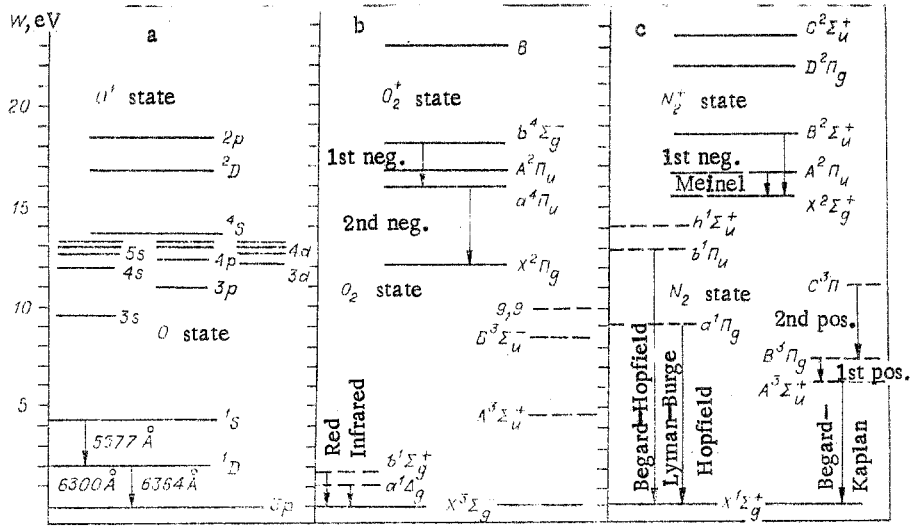

Fig. 1

The absorber was considered to be a stratified-homogeneous medium consisting of a mixture of atomic oxygen (OI), molecular oxygen, and molecular nitrogen, with the in-depth distribution of the concentrations of these gases following an exponential law. Such a distribution, for an appropriate choice of exponent parameters, enables us to simulate natural media, such as planetary atmospheres. In the case of specific calculations for the earth (see below), the parameters of the concentration distributions for the above-mentioned components of the mixture were chosen in accordance with the CIRA-65 neutral-atmosphere model [6] with an exospheric temperature of 1000°K. We considered both elastic scattering and OI transitions for O_2 and N_2 into the excited states of the discrete spectrum (characteristic excitation) and the continuous spectrum (ionization). The atomic oxygen was described as a system capable of being excited in 15 triplet states of the discrete spectrum with a configuration of the form $1S^22S^22p^3(^4S)nl$ (nl = 3s – 8s, 3p – 6p, 3d – 7d) into two metastable states ^1D and ^1S of the fundamental configuration and three ionization states ^4S, ^2P, and ^2D. The molecular oxygen was described by three forbidden transitions into the $a^1\Delta g$, $b^1\Sigma_g^+$, and $A^3\Sigma_g^-$ states, two allowed transitions with maxima in the absorption sectra centered at 8.4 and 9.9 eV, and five ionization states $X^2\Pi_g$, $a^4\Pi_u$, $A^2\Pi_u$, $b^4\Sigma_g^-$. The molecular nitrogen was represented by four forbidden transitions into the $A^3\Sigma_u^+$, $B^3\Pi_g$, $a^1\Pi_g$, $C^3\Pi_u$ states, two allowed transitions with maxima in the absorption spectra centered at 12.85 and 14.0 eV, and five ionization states $X^2\Sigma_g^+$, $A^2\Pi_u$, $B^2\Sigma_u^+$, $D^2\Pi_g$, $C^2\Sigma_u^+$. In addition to the partial cross sections of excitation, we also used the total integral cross sections of scattering in blocks such as those used in the determination of the free path length or the kind of gas doing the scattering. The simplified scheme of the main OI terms for O_2 and N_2 is shown in Fig. 1. All the differential and integral cross sections of interaction used were introduced directly into the program in analytic form, in accordance with the results of [7-10]. A detailed description of the physical medium and the algorithm used in this study for simulating the electron trajectories is given in [11].

The calculations were carried out for electron beams with initial normal angles of incidence to the absorber surface and initial energies in the E_0 = 0.1-1-keV range. The trajectories were simulated on the M-4030 computer; 6000 trajectories were simulated, which ensured a statistical error of no more than 10% with a confidence limit of 0.95.

Penetration Characteristics. For the investigation of the connection between the initial parameters of the electron beam and its path length, we calculated the penetration curves, or, as they are sometimes called, the transmission coefficients T_N for a number of particles:

$$T_N(z) = n(z)/N,$$

where n(z) is the number of particles from the primary beam of intensity N whose depth of transverse penetration (along the normal to the surface of the medium) is equal to the mass z. Figure 2 shows examples of T_N (dots) calculated for electrons with initial energies of E_0 = 0.1, 0.15, and 0.2 (curves 1-3, Fig. 2a) and 0.4, 0.6, 0.8, and 1 keV (curves 1-4, Fig. 2b). As the analysis showed, the curves of transmission of low-energy electrons in a gaseous

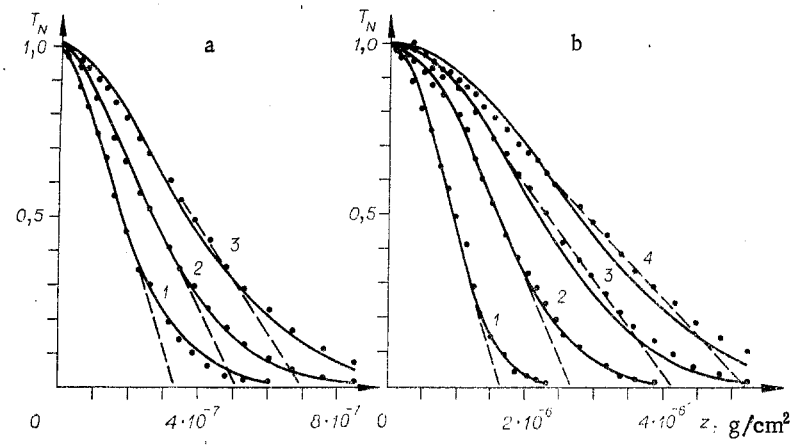

Fig. 2

medium in the case of normal incidence to the surface of the absorber, just as in the case of their transfer in massive solid targets, satisfy the following empirical law:

$$T_N(z) = \exp\left[-\alpha(E_0)\, z^{p(E_0)}\right]. \quad (1)$$

The curves calculated by formula (1) are shown in Figs. 2a, b as solid curves. The coefficients $\alpha(E_0)$ and $p(E_0)$ were determined by the least-squares method. In Fig. 3 we have constructed the graphs of α and p (curves 1 and 2) as functions of the initial electron energy; from the shape of the curves it follows that in the interval from 0.1 to 0.5 keV, p and α increase monotonically. However, while p approaches a constant value equal to 2.1, α reaches a maximum in the 0.4-0.6-keV region and then begins to decrease as E_0 continues to increase. Here (E_0 > 0.5 keV) the behavior of α is approximated fairly well by a power function of the form

$$\alpha(E_0) = 3.2\cdot10^{11} E_0^{-3.32}. \quad (2)$$

The results were found to be in good agreement with the data of experimental measurements of T_N for electrons with E_0 > 0.6 keV carried out with massive specimens of aluminum (z_{Al} = 13) and silicon film (z_{Si} = 14). Thus, the parameter p calculated in [1, 3] was found to be 1.8 and 2.1 for Al and Si, respectively. The law obtained in the form of (1) can be explained if we assume that the differential law of attenuation of the electron beam in a massive gas mixture has the form

$$-dT_N(z)/T_N = \gamma z^s dz. \quad (3)$$

Integrating (3) and taking account of the boundary conditions $T_N(z = 0) = 1$, we immediately obtain (1), where $p = 1 + s$, $\alpha = \gamma/p$.

Integral Path Lengths. In the current literature we encounter four "types" of integral path lengths: the total path length, R_{tot}; the extrapolated (practical) path length, R_{ext}; the normal path length, R_e; and the average path length, $\bar{R}$. The basis for determining all the above path lengths is provided by the curves of T_N, describing the value of the intensity (based on the relative number of particles) of the electron beam, depending on the mass of absorber it has penetrated. By the total path length R_{tot} we usually mean the maximum depth of penetration of the electrons. However, since $T_N(z)$ tends to zero asymptotically, it is fairly difficult to determine unambiguously the depth of maximum penetration of the electron beam into the absorber and to estimate the accuracy of the resulting value. The method used for determining the total path length is itself more a geometric than a physical method. The same defect is found in the method of determining the extrapolated path lengths. On the curve of $T_N(z)$ we try to distinguish a segment which is nearly a straight line. Extrapolation of this quasilinear segment until it intersects the abscissa axis yields the value of the mass which is called the extrapolated path length. On the other hand, the concepts of normal and average path length are rigorously defined physical quantities. By the normal path length we mean the value of the mass such that after passing through this mass the intensity of the beam decreases by a factor of e. The average path length is the mathematical expectation of the density of distribution of the path lengths of the primary electrons

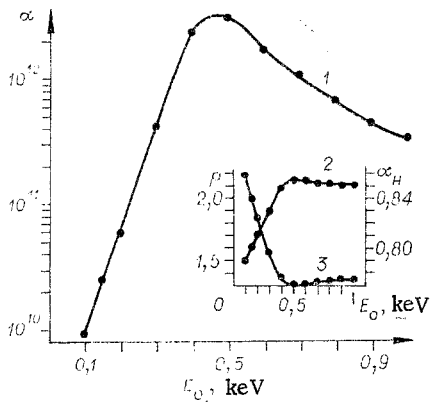

Fig. 3

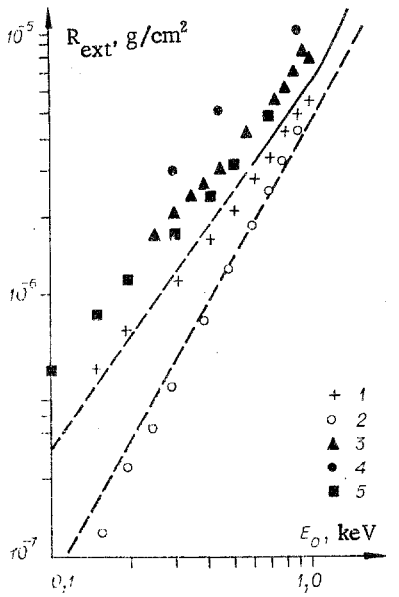

Fig. 4

$$\bar{R} = \int_0^\infty z \frac{\partial T_N(z)}{\partial z} dz \Big/ \int_0^\infty \frac{\partial T_N(z)}{\partial z} dz. \tag{4}$$

Even though the determination of the extrapolated path length is more a graphical than a physical one and involves considerable arbitrariness, we shall discuss it in more detail, because a large proportion of the experimental data in the literature are presented in terms of extrapolated path lengths. We consider Fig. 2a, b, where the dashed curves are examples of the extrapolation of quasilinear segments of T(z) to an intersection with the z-axis, which corresponds to the method of determination of the extrapolated path lengths. Figure 4 shows the values of R_{ext} calculated in this way (these are the points marked 1, while the points 2-5 are the results of [12-15]) and also shows the results of a number of experimental measurements of what might be covered by the concept of extrapolated path lengths. Here the dashed curve shows the functional relation (extrapolated from the region $E_0 > 5$ keV) between the initial energy E_0 and the extrapolated path length R_{ext} which is most often used in applied problems, a relation obtained by Grün [16]:

$$R_{ext} = 4.57 \cdot 10^{-6} E_0^{1.75} \quad (5 < E_0 < 54), \tag{5}$$

where E_0 is given in keV and R_{ext} is given in g/cm². The observed agreement between the results of [12] and function (5) extrapolated into the region $E_0 < 1$ keV cannot serve as proof that relation (5) can justifiably be carried over from the high-energy region to the region of energies below 1 keV. As was shown in a critical survey [17], the results of [12, 14] are erroneous and cannot be used to establish a connection between the initial energy and the integral path length of the electron. The extrapolated path lengths which we calculated are closer to the results of [13, 15] (the points 3, 5), but in these experiments it is not clear how close the measurement conditions were to the conditions in thick targets. In connection with this, it is of considerable interest to compare the path lengths obtained above with the results of [1, 2], which reported measurements of the penetration coefficient T_N of electrons with energies of $E_0 > 0.6$ keV into the thickness of a massive aluminum target by the film-block method. It should be noted that in these experiments the charge numbers of the material of the target were close to the actual charge number of the model of the absorber (model of the atmosphere) used in the present paper. The extrapolated path lengths calculated on the basis of the T_N penetration curves given in [1, 2] are shown in Fig. 4 by a solid curve; the dashed line is the extrapolation of these calculations to the energy range below 0.6 keV. It should be noted that there is good agreement between the R_{ext} values calculated on the basis of numerical simulation (the points 1) with the R_{ext} values calculated on the basis of the data of [1, 2]. As noted above, the most physical and most unambiguously defined path lengths are the average and normal path lengths. Using the representation (1), we can find the average path length from formula (4):

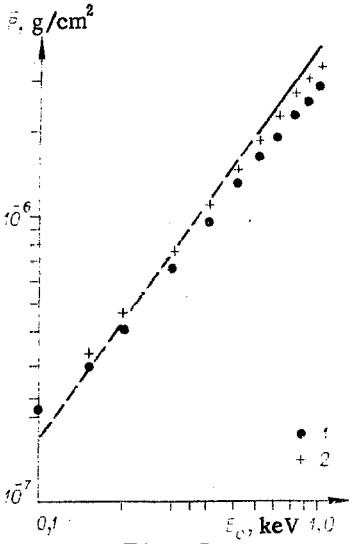

Fig. 5

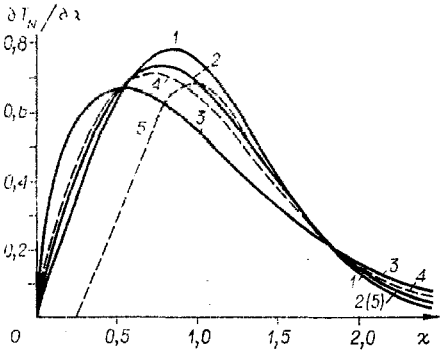

Fig. 6

$$\bar{R} = \int_0^\infty z \frac{\partial T_N(z)}{\partial z} dz = \frac{\Gamma(1+1/p)}{\alpha^{1/p}}, \tag{6}$$

where $\Gamma(1 + 1/p)$ is the gamma function. The average path lengths obtained by (6) are shown in Fig. 5 (the points 1). The solid curve shows the variation of $\bar{R}$ as a function of E_0 obtained for electron transfer in massive aluminum in [1, 2], and the dashed line is the extrapolation of the experimental graph into the region $E_0 < 0.6$ keV; the points z are the normal path lengths. Making use of (6) and the analytic representation of $\alpha(E)$ in the form (2), we can express $\bar{R}$ for $E_0 > 0.6$ keV as

$$\bar{R}(E_0) = 3.32 \cdot 10^{-6} \Gamma(1+1/p) E_0^{3.32/p(E_0)}.$$

Then for p = const we obtain the same power function of E_0 characterizing $\bar{R}$ that is characteristic of the analytic representations of integral path lengths for small energy intervals of variation of E_0 both in the high-energy and in the low-energy range.

Dispersion of Path Lengths. The family of curves $T_N(z)$ can be represented in normalized form. Such a representation of $T_N(z)$ ensures that the results will be written in a form suitable for comparison with the data of experiments with different targets. Choosing as the normalizing parameter the average path length R_0 and substituting (6) into (1), we obtain

$$T_N(\chi) = \exp\left[-\alpha_H(E_0)\chi^{p(E_0)}\right], \tag{7}$$

where $\alpha_H(E_0) = [\Gamma(1 + 1/p)]^p$; $\chi = z/\bar{R}$.

From the nature of the behavior of the parameters p and α_H, depending on the initial energy E_0, an illustration of which is shown in Fig. 3 (curves 2 and 3), it follows that the law governing the decrease in intensity of the electron beam for $E_0 > 0.6$ keV, shown in the normalized form (7), is independent of the energy of the primary beam.

Differentiation of the $T_N(z)$ curve gives us the path-length distribution known as the dispersion of the path lengths. Differentiating the normalized $T_N(\chi)$, we obtain the dispersion curves for the path lengths in normalized form, which are shown in Fig. 6 for $E_0 > 0.6$ keV and $E_0 = 0.3$ and 0.1 keV (curves 1-3, respectively), and curves 4 and 5 represent the normalized densities of distribution of the path lenghts obtained in [1-3] by the method of shooting through massive bodies and free films made of Al for $E_0 > 0.6$ keV. It should also be noted that the density of distribution of the path lengths in a massive target is substantially different from the analogous distribution obtained in experiments with thin films. The maximum of $\partial T_N(\chi)/\partial\chi$, formed by scattering in thin films (curve 5), is displaced toward larger values of χ more than the corresponding maximum of the path-length distribution in a massive solid (curve 4). We observe a considerable reduction in the proportion represented by small path lengths in thin films in comparison with a massive absorber. Therefore, in the solution of specific applied problems, e.g., those connected with the transfer of electron beams in the atmosphere of the earth, it must be borne in mind that the atmosphere constitutes a typical massive absorber and that the use of experimental data on the characteristics of the interaction of electrons with thin films may lead to considerable errors.

TABLE 1

E_0, keV	p	α	α_H	R_{ext}, g/cm²	R_e, g/cm²	$\bar{R}$, g/cm²
0,1	1,5	9,04(9)*	0,858	3,5(—7)	2,3(—7)	2,08(—7)
0,15	1,6	2,30(10)	0,839	5,15(—7)	3,35(—7)	2,99(—7)
0,2	1,7	6,05(10)	0,824	7,15(—7)	4,65(—7)	4,06(—7)
0,3	1,9	4,26(11)	0,797	1,17(—6)	7,85(—7)	6,72(—7)
0,4	2,08	2,40(12)	0,777	1,67(—6)	1,12(—6)	9,89(—7)
0,5	2,15	3,20(12)	0,770	2,12(—6)	1,5(—6)	1,35(—6)
0,6	2,14	1,78(12)	0,771	2,76(—6)	1,87(—6)	1,67(—6)
0,7	2,13	1,10(12)	0,772	3,40(—6)	2,32(—6)	1,94(—6)
0,8	2,12	6,92(11)	0,773	4,15(—6)	2,77(—6)	2,33(—6)
0,9	2,11	4,61(11)	0,774	4,72(—6)	3,16(—6)	2,58(—6)
1,0	2,1	3,20(11)	0,775	5,25(—6)	3,47(—6)	2,94(—6)

*9.04(9) = $9.04 \cdot 10^9$

The above parameters p, α, α_H of the penetration curves and the calculated integral path lengths (R_{ext}, R_e, $\bar{R}$) for electron beams with initial energies of E_0 = 0.1-1 keV and initial pitch angles θ_0 = 0 (perpendicular incidence on the absorber surface) are shown in Table 1.

The authors wish to express their gratitude to G. V. Starkov for his valuable comments on the work and to L. K. Khvostenko for assistance in performing the calculations.

LITERATURE CITED

1. A. Ya. Vyatskii and V. Yu. Khramov, "Method for determining the characteristics of the interaction of medium-energy electrons with massive solids," Fiz. Tverd. Tela, 17, 3412-3413 (1975).
2. A. Ya. Vyatskii and V. Yu. Khramov, "Laws governing the interaction of medium-energy electrons with massive solids," Fiz. Tverd. Tela, 17, 3432-3434 (1975).
3. A. Ya. Vyatskii and V. Yu. Khramov, "Energy distribution of electrons passing through thin films of silicon and gold," Fiz. Tverd. Tela, 16, 1818-1820 (1974).
4. A. A. Belyaev and A. I. Krupman, "Estimate of the applicability of a theory in the problem of the penetration of a charged particle through a layer," At. Energ., 35, 95-100 (1973).
5. L. Landau, "On energy losses of fast particles by ionization," J. Phys. USSR, 8, 204-205 (1944).
6. CIRA-1965, North-Holland, Amsterdam (1965).
7. A. E. S. Green and R. S. Stolarski, "Analytical models of electron impact excitation cross sections," J. Atmos. Terr. Phys., 34, 1703-1717 (1972).
8. V. E. Ivanov, N. K. Osipov, and V. A. Shneider, "Analytic representation of the cross sections of elastic scattering of low-energy electrons by atmospheric gases," Geomagn. Aeron., 17, 242-245 (1977).
9. V. E. Ivanov, N. K. Osipov, and V. A. Shneider, "Integral cross sections of scattering of low-energy electrons by atomic oxygen," Geomagn. Aeron., 17, 472-477 (1977).
10. V. E. Ivanov and N. K. Osipov, "Integral cross section of scattering of low-energy electrons (E < 1 keV) by atmospheric gases," Preprint No. 15 (189), IZMIRAN, Moscow (1977).
11. V. E. Ivanov, N. K. Osipov, G. V. Starkov, and L. K. Khvostenko, "The Monte Carlo method in problems involving the transfer of low-energy electrons (E < 1 keV) in the atmosphere," in: Polar Auroras [in Russian], Nauka, Moscow (1979).
12. G. Anslow, "The total ionization produced in air by electrons of various energies," Phys. Rev., 25, 484-500 (1925).
13. J. F. Lehmann and T. H. Osgood, "The total ionization due to the absorption in air of slow cathode rays," Proc. R. Soc., 115, 609-624 (1927).
14. J. R. Young, "Penetration of electrons in aluminum oxide films," Phys. Rev., 103, 292-293 (1956).
15. P. L. Hartman, "New measurements of the fluorescence efficiency of air under electron bombardment," Planet. Space Sci., 16, 1325-1340 (1968).

16. A. E. Grün, "Lumineszenz-photometrische Messungen der Energieabsorption im Strahlungsfeld von Elektronen-Quellen eindimensionaler Fall in Luft," Z. Naturforsch., 12a, 89-95 (1957).
17. J. A. Gledhill, "The range-energy relation for 0.1-500-keV electrons," J. Phys., A6, 1420-1428 (1973).

OPTIMIZATION OF THE WORKING CONDITIONS IN AN ACCELERATOR WITH AN ANODE LAYER

V. S. Erofeev,* V. P. Naumkin, and I. N. Safronov

UDC 629.7.036.74

The characteristics of a two-stage ion accelerator with an anode layer [1, 2] indicate that there are at least two modes of operation: accelerative and anomalous. The occurrence of the anomalous state substantially restricts the performance of the accelerator. It is therefore extremely important to elucidate (at least qualitatively) the main factors that influence the change of mode. An experimental study has been made of the effects of the geometry of the working part on the characteristics, and a relationship is drawn up between the parameters and the working conditions at the limit of transition from the optimum accelerative mode to the anomalous one. The experiments were performed on a two-stage axial ion accelerator with an anode layer [1].

1. Effects of Working-Gap Geometry on Accelerator Characteristics. An accelerator with an anode layer usually works with a strong magnetic field in the working gap, $H \gtrsim 1000$ Oe. The thickness of the accelerating anode layer is considerably less than the thickness of the region where the ion beam propagates transverse to the magnetic field. The extent of this region is determined by the distance from the end of the discharge stage to the end of the magnetic system and by the zone of the leakage field, which is of the order of the distance between the poles. The electrons have a restricted mobility transverse to the magnetic field, so the space charge due to the ion beam in the magnetic field is compensated only by ionization of the residual gas and the possible entry of electrons along the magnetic field lines. Under these conditions, dynamic processes in the beam may lead not only to deterioration in the parameters but also to periodic beam shutdown [3-5]. It is therefore important to establish the relationship between the characteristics of the accelerator and the extent and geometry of the region containing the magnetic field.

Figure 1 shows the voltage–current characteristics of accelerating stages differing in magnet geometry and thus in geometry of the acceleration chamber (V_d = 150-200 V, H = 2 kOe, and $p = (2\text{-}4)\cdot10^{-5}$ mm Hg). In the first case (Fig. 1a), the magnet has thick poles (40 mm) with a wide spacing (50 mm). The discharge unit is set up in the pole space with the accelerating layer essentially in a uniform magnetic field. The optimum acceleration conditions (with $I_a \simeq \text{const} \simeq \dot{e}m/M$, where $\dot{m}$ is the flow rate of working substance per second, M is the mass of an atom, and e is the charge on an ion) occurs only for $V_a \gtrsim 3\text{-}4$ kV. The negative slope of the voltage–current characteristic is very large at low V_a, so it is possible to follow the course of the characteristic in this region only for $I_a \gtrsim 3$A. As V_a is reduced, there is a step change from the optimum acceleration condition to a comparatively low-voltage condition, which is called anomalous, because the current in the accelerating stage may exceed the possible ion current considerably ($I_a > \dot{e}m/M$), while the formation of the ion beam deteriorates considerably. We take the critical voltage V_a^* for the transition to the anomalous state as the accelerating potential at the point where the slope of the voltage–current characteristic becomes negative or there is a jump from the accelerating condition to the anomalous one.

When the geometry of the accelerator is changed (Fig. 1b and c), the poles become considerably thinner, while the distance between them is reduced by more than a factor of 2. As a result, the length of the region where the ion beam propagates across the magnetic field is

*Deceased.

Kaliningrad, Moscow Region. Translated from Zhurnal Prikladnoi Mekhaniki i Tekhnicheskoi Fiziki, No. 1, pp. 27-34, January-February, 1981. Original article submitted November 13, 1979.

 0021-8944/81/2201-0022$07.50